Featured in Physics

## Reconnection-Powered Fast Radio Transients from Coalescing Neutron Star Binaries

Elias R. Most<sup>1,2,3,\*</sup> and Alexander A. Philippov<sup>4</sup>

<sup>1</sup>Princeton Center for Theoretical Science, Princeton University, Princeton, New Jersey 08544, USA <sup>2</sup>Princeton Gravity Initiative, Princeton University, Princeton, New Jersey 08544, USA <sup>3</sup>School of Natural Sciences, Institute for Advanced Study, Princeton, New Jersey 08540, USA <sup>4</sup>Department of Physics, University of Maryland, College Park, Maryland 20742, USA



(Received 28 July 2022; revised 28 February 2023; accepted 17 April 2023; published 16 June 2023)

It is an open question whether and how gravitational wave events involving neutron stars can be preceded by electromagnetic counterparts. This Letter shows that the collision of two neutron stars with magnetic fields well below magnetar-level strengths can produce millisecond fast-radio-burst-like transients. Using global force-free electrodynamics simulations, we identify the coherent emission mechanism that might operate in the common magnetosphere of a binary neutron star system prior to merger. We predict that the emission show have frequencies in the range of 10-20 GHz for magnetic fields of  $B^* = 10^{11}$  G at the surfaces of the stars.

DOI: 10.1103/PhysRevLett.130.245201

Introduction.—Gravitational wave events involving the collision of two neutron stars [1,2], are a rich playground for multimessenger astronomy [3,4]. They a broad range of transients in the optical and infrared [5-11], gamma-[12,13], and x-ray [14–17], as well as radio [18–22] bands. While at present it has only been possible to detect gravitational waves emitted during the inspiral of two neutron stars, the above electromagnetic transients are thought to be sourced during the merger and post-merger phase, respectively during and after the collision (see, e.g., [23,24] for recent reviews). On the other hand, the presence of potentially strong magnetic fields in neutron stars has led several studies to propose that there might be yet another electromagnetic counterpart, that—different from the others—would be sourced prior to merger. Such an event is commonly referred to as an electromagnetic precursor. In fact, recent (indirect) observational evidence has pointed towards the existence of such precursor events [25], which additionally claimed the presence of magnetar-level field strengths in the inspiraling system. Typical models generally have predicted emission across the entire electromagnetic spectrum involving gammaray [26-28], radio [29-32], and/or x-ray transients [33]. While these models have mostly been analytical, a number of studies have attempted to numerically model various global scenarios producing these transients. They include emission associated with the motion of the neutron stars [34], flares in the magnetosphere [35,36] (see also [33,37]), dissipation in the common magnetosphere of the two stars [38–40], or balding of the black hole formed in a prompt collapse scenario [41] (see also [42–46]). Similar numerical studies have also been performed for black hole—neutron star systems [47–49].

Different from all previous studies—analytical and numerical—here we utilize the three-dimensional dynamics modeled in global simulations of the common magnetosphere to clearly establish which coherent emission mechanism is likely operating, and under what conditions. We demonstrate, for the first time, that electromagnetic flares emitted prior to merger can interact directly with the current sheets present in the binary's magnetosphere, causing large scale reconnection in the compressed orbital current sheet. Leveraging state-of-the-art models for linearly polarized fast radio bursts (FRBs) [50,51], we robustly link the interaction dynamics inside the common binary magnetosphere to an FRB-like millisecond transient at frequencies of 10-20 GHz.

Results.—In the following, we describe a novel mechanism capable of producing fast radio transients prior to the merger of two neutron stars. This reconnection-driven mechanism originates from the interaction of electromagnetic flares with the common binary neutron star magnetosphere. We proceed in three steps. First, we utilize global force-free electrodynamics simulations to study a binary neutron star system featuring spinning stars with misaligned magnetic moments. Such an approach is appropriate to capture the dynamics of the highly conducting pair-plasma-filled binary magnetosphere [52-54] (see the Appendix for details). Second, based on the simulation outcome we identify the likely candidate for a coherent radio emission mechanism. Finally, we use insights gained from previous kinetic simulations and analytic theory associated with the mechanism to predict the emission consistent with condition probed in our global simulations.

We begin by illustrating the flaring mechanism and its interaction with the orbital current sheet. Neutron star binaries with oppositely oriented magnetic moments can feature connected magnetic flux tubes [55,56]. Relative motion between the two stars, i.e., orbital motion or stellar spin, can lead to a twisting of those flux tubes. Once overtwisted, the connected field lines will snap and release a strong magnetic bubble [35]. In an earlier work [36], we have shown that this mechanism is relatively insensitive to the precise field geometry, strength or alignment, as long as the overall topology (magnetic moments pointing in opposite hemispheres) is preserved. Generically these flares can feature bulk Poynting fluxes of  $> 10^{42}$  erg/s for field strengths  $B \sim 10^{11}$  G.

While the mechanism can in principle operate earlier, the flaring strength will only become observationally relevant in the final second before the collision [35,36]. Crucially, the missing component in these studies has been the identification of a self-consistent emission mechanism applicable to this system. To alleviate this, it is necessary to track the subsequent evolution of the flare after it has been launched from the two stars. For ease of demonstration, we first focus on an idealized system consisting of two perfectly antialigned magnetic dipoles, with one of them being 50× less strong than the other. In the second step, we will focus on a more realistic system. Starting with the left panel of Fig. 1, we can see that the relative orbital motion induces a twist of the connected flux tubes, leading to the emission of two flares. Because of the unequal field strengths of the dipoles, the flares are strongly beamed towards the orbital plane [36]. They will ultimately hit the orbital current sheet and enhance reconnection (right panel). We can see that the latter leads to the appearance of plasmoids (magnetic islands), the merger of which is associated with the production of low-frequency radiation [57,58]. While the properties of the emission will strongly depend on the ratio of the magnetic field strength in the flare to the background field in the current sheet, a similar mechanism has been proposed to explain linearly polarized FRBs from active magnetars [50]. In the following, we will demonstrate that the same scenario naturally arises in generic binary configurations. In the third step, we will use those to infer the properties of the resulting emission.

We now focus on a more realistic system, where one of the neutron stars is rapidly counter-spinning and has an

inclined magnetic field. Although most neutron star binaries are thought to be nearly irrotational [59], we specifically pick this configuration as it leads to a submillisecond periodicity, potentially relevant for FRB20201020A-type events [60]. More specifically, in Fig. 2 we consider the evolution in the orbital plane showing both the magnetic field strength  $\sqrt{B^2}$  and the squared current density  $\mathcal{J}_{\mu}\mathcal{J}^{\mu}$ . Since the flaring happens periodically with a combination of the orbital and spin period of the stars [37], this will highlight the propagation of the flares. During the time interval shown, two flares will be emitted, although we will largely focus on the first flare only. For clarity, we have labeled them as *flare* 1/2. Tracking their evolution in time, we can identify three different phases: pre-interaction (left panel), interaction (middle panel) and post-interaction phase (right panel) with the highlighted part of the orbital current sheet. Concentrating at the magnetic field strength, we can follow the propagation of flare 1. After its inception it expands and approaches the orbital current sheet. We point out that since the simulations have been performed in the corotating frame, the flares have a counter-clockwise outwards spiralling motion in this depiction. Once the flare reaches the highlighted part of the current sheet, we can see that the dissipation is locally enhanced. This is most easily visible in the bottom row, which indicates the (complex) current sheet structures. We can see that the interaction is associated with a compression of the current sheet. Finally, after the flare has propagated past the sheet, small magnetic islands (plasmoids) begin to appear (right column). They can be seen as local overdensities (bright spots) both in the magnetic field strength,  $\sqrt{B^2}$ , and in the co-moving current density,  $\sqrt{\mathcal{J}_{\mu}\mathcal{J}^{\mu}}$ . In fact, due to the periodic emission of flares, multiple interactions of flares with different parts of the orbital current sheet will locally produce plasmoids throughout the domain, as can be seen in the little bright spots present at all three times shown in Fig. 2. Some of those have already begun to merge, although their physical size and full dynamics cannot be captured with the forcefree approach adopted in this work. Nonetheless, our simulations clearly establish the viability of the current

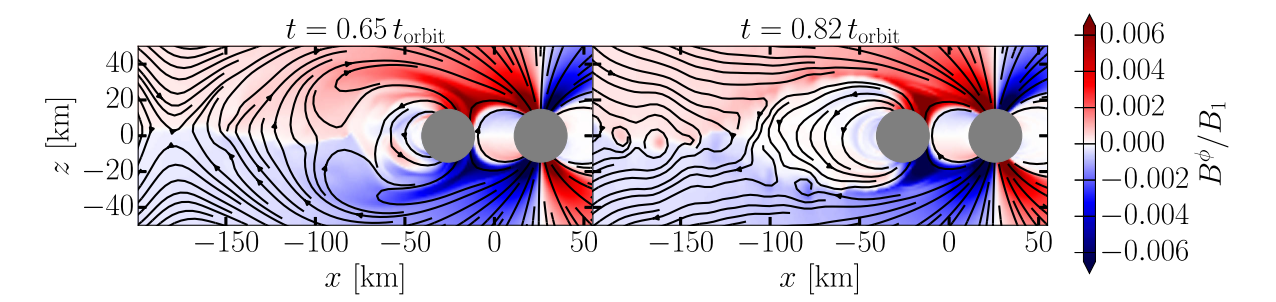


FIG. 1. Representative interaction of electromagnetic precursor flares with the orbital current sheet (at z=0 km) for counteraligned dipoles. (Left) Launching of the flares from overtwisted flux tubes. (Right) Reconnection in the current sheet and the formation of plasmoids. Shown in color is the out-of-plane component  $B^{\phi}$  of the magnetic field, which indicates the twist in the magnetosphere. The times are shown relative to the orbital period,  $t_{\text{orbit}}$ , and field strength values are stated relative to the value  $B_1$  at the surface of the right star.

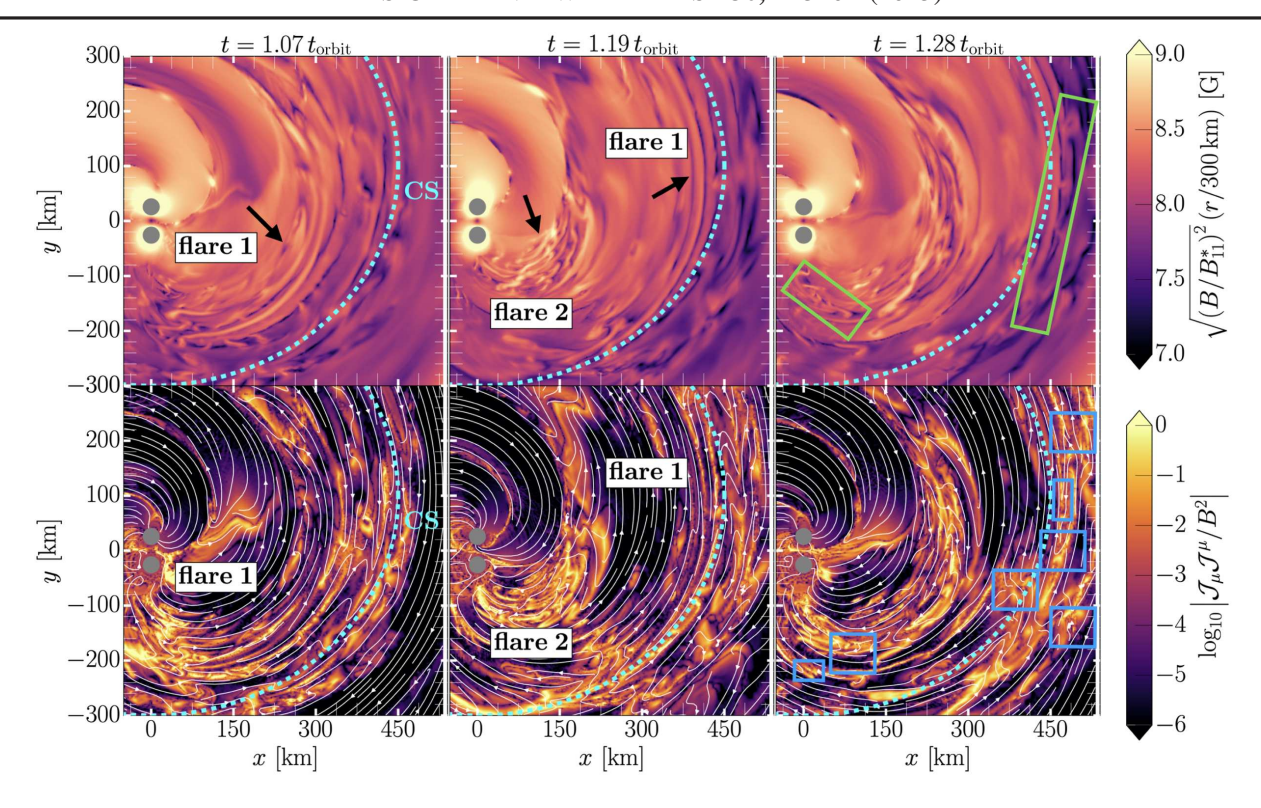


FIG. 2. Interaction of electromagnetic precursor flares with the orbital current sheet (CS) in the orbital plane. A sequence of two flaring events is shown. As the flares propagate outwards they interact with the orbital current sheet. For clarity, only one stripe has been marked using a dashed cyan line. The top row shows the total magnetic field strength,  $\sqrt{B^2}$ , rescaled by the cylindrical radius, r, and magnetic field strength,  $B_{11}^*$ , (in units of  $10^{11}$  G) at the surface of the stars. The bottom row shows the magnitude of the electric four-current,  $\mathcal{J}^{\mu}$ , highlighting the current sheet. The interaction process triggers reconnection that leads to the formation of plasmoids (magnetic islands), some of which are highlighted by a green box. Flare-induced reconnection x-points are highlighted by blue boxes. All times t are stated relative to the orbital period,  $t_{\text{orbit}}$ . A movie version of this figure is available online as supplemental material [62].

sheet-flare interaction mechanism outlined above. In fact, the authors are not aware of a global simulation demonstrating this mechanism even for an isolated star (see Ref. [51] for a local simulation of the interaction itself). In order to better demonstrate the flare-current sheet interaction, Fig. 3 shows an enlarged rendering of a flare hitting the orbital current sheet. Both the toroidal field structure of the flare and the deformation of the current sheet are clearly visible. Subsequently, the flare drags along the orbital current sheet, compressing it and causing it to reconnect on large (angular) scales. This implies that the emission caused by the merger of plasmoids will likely cover a large spatial volume, enhancing its detection prospects greatly [61].

Emission process.—In the following, we want to characterize the emission we expect as a result of the current sheet-flare interaction. This entails estimating luminosity, duration and frequency of the event. To do so, we will combine global numerical findings, i.e., magnetic field strengths, spatial flare extent and duration, with analytical expression for the small-scale plasma physics processes not captured by the simulations [50,51]. This way we are able to model unresolved reconnection microphysics not captured by artificial dissipation in our force-free approach. We

start out by describing the luminosity and event duration. Figure 4 shows the Poynting flux luminosity associated with the flares,  $\mathcal{L}_{EM}$ , and the dissipative luminosity,  $\mathcal{L}_{diss}$ , associated with reconnection (see Ref. [36] for details on how to compute these quantities). We can see that periodic flaring is present, with about four flares being emitted per orbit. The exact periodicity can be computed based on topological arguments [37]. We point out that this rapid periodicity is a result of having counterspinning stars in the binary, making it suitable to produce observable sub-ms variability. Overall we find that  $\mathcal{L}_{\rm EM} \simeq 10^{42} (B_{11}^*)^2 \ {\rm erg/s}$  and  $\mathcal{L}_{\rm diss} \simeq -3 \times 10^{41} (B_{11}^*)^2 \ {\rm erg/s}$ , where  $B_{11}^*$  is the value of the strength of the field at the stellar surface in units of 10<sup>11</sup> G. We point out that the physical Lundquist number associated with this dissipation will be high so that reconnection will happen in the plasmoid regime [63,64]. From Fig. 3 we read off a light-crossing time across a flaring electromagnetic bubble of  $\tau \simeq 0.3$  ms. From Fig. 2 we infer that the magnetic field strength in the flare at the light cylinder,  $B_{\text{flare}} \simeq 8 \times 10^8 B_{11}^*$  G, is about 20 times stronger than the field strength in the binary wind,  $B_{\text{wind}}$ . The Lorentz factor of the plasma in the flaring pulse can be estimated as [50],  $\Gamma = \sqrt{B_{\rm flare}/B_{\rm wind}}/2 \approx 2.2$ . When the

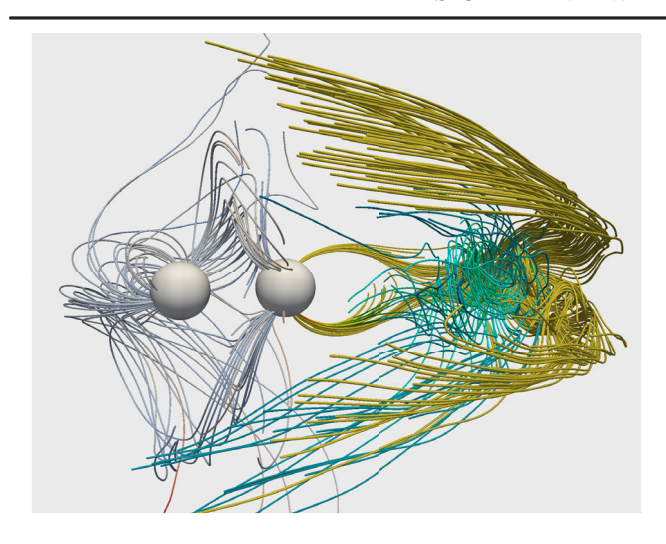


FIG. 3. Enlargement: selected magnetic field lines of the flare (blue) interacting with field lines of the orbital current sheet (yellow) at time  $t \simeq 1.18 t_{\rm orbit}$ . The field lines in the flare are predominantly toroidal, which begins to get compressed during the impact. For illustration purposes, only a subset of the magnetic field lines is shown.

flare arrives at the current sheet, it triggers violent compression and reconnection. This is different from intrinsic tearing of the elongated sheet in the quiescent binary magnetosphere, which alone is not energetic enough to produce observable transients (and at lower frequencies than in a compressed sheet). The magnetic flux in the pulse is comparable to the flux within the stripe of the binary wind,  $\phi_{\text{flare}}/\phi_{\text{wind}} \sim B_{\text{flare}}/B_{\text{wind}}(c\tau/R_{\text{LC}}) \approx \text{few}$ , where  $R_{\rm LC}$  is the light cylinder of the binary. In this case, local kinetic simulations of pulse-current sheet interactions [51] show that the dissipated power is of order of  $\mathcal{E}_{diss}$  ~  $\beta_{\rm rec} L_{\rm EM} \tau$ , where  $\beta_{\rm rec} \approx 0.1$  is the dimensionless rate of magnetic reconnection (e.g., [65-67], see also [68,69]). For our scenario, this results in  $\mathcal{E}_{\rm diss} \approx 10^{38} (B_{11}^*)^2$  erg. The tearing-mode instability results in the current sheets fragmentation into a sequence of magnetic islands, and their collisions source low-frequency fast magnetosonic waves [57,58]. Simulations show that a fixed fraction of the power dissipated in the reconnection,  $f \approx 2 \times 10^{-3}$ , gets converted into the low-frequency radiation [51,58]. For the luminosity we then obtain  $\mathcal{L}_{\text{radio}} \approx 0.1 f L_{\text{EM}} \approx$  $2 \times 10^{38} (B_{11}^*)^2$  erg/s. The observed signal duration is of order of a light-crossing time across a flaring bubble [51],  $\sim \tau \simeq 0.3$  ms, and, hence, can give rise to sub-millisecond transients [60].

In the next step, we need to establish that this reconnection-powered transient indeed occurs in the radio band. In the reference frame of the pulse, the characteristic frequency of the emission associated with the merger of plasmoids,  $\nu' = c/(2\pi\zeta d'_{\rm plasmoid})$ , is determined by the sizes of typical plasmoids in the chain,  $d'_{\rm plasmoid} = \xi r_L$ , where  $r_L = m_e c^2 \langle \gamma \rangle / (e B'_{\rm flare})$  is the Larmor radius of the

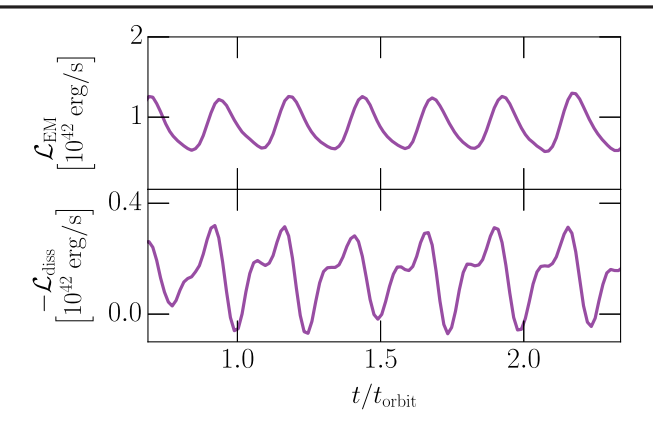


FIG. 4. Electromagnetic power,  $\mathcal{L}_{EM}$ , of the outgoing flare (top), and (approximately) dissipated power,  $\mathcal{L}_{diss}$ , in the current sheet (bottom). These have been normalized for a  $B^* \sim 10^{11}$  G magnetic field at the surface of the stars. All times are stated relative to the orbital period,  $t_{orbit}$ .

particles heated by reconnection up to averaged Lorentz factor  $\langle \gamma \rangle$ , and  $\zeta \approx 1$ ,  $\xi \approx 10$ –100 are numerical factors. These length scales cannot be resolved in our global force-free simulations, and would, in fact, require full kinetic simulations. However, local small-scale simulations performed in the regime of very fast synchrotron losses, applicable to the binary magnetosphere, find a balance between particle energization by reconnection and synchrotron cooling. This results in  $\langle \gamma \rangle \approx \gamma_{\rm rad} = \sqrt{3e\beta_{\rm rec}B'_{\rm flare}/(2r_e^2B'_{\rm flare})}$  (e.g., [51]). Following results of kinetic simulations [51], we adopt  $\xi \zeta \approx 90$ . Transforming into the lab frame, this implies a frequency of the transient [50,51],

$$\nu_{\text{FRB}} = \frac{1}{2\pi\xi\zeta} \sqrt{\frac{2r_e}{3\beta_{\text{rec}}c\Gamma}\omega_B^3} \simeq 16 \ (B_{11}^*)^{3/2} \text{ GHz},$$
(1)

where  $\omega_B = eB_{\rm flare}/m_e c$  is the electron gyrofrequency in the pulse frame, for the emission of fast radio transients from the late inspiral of neutron star binaries. For varying parameters of the binary, this frequency may decrease by a factor of a few, if the collision of the pulse and current sheet happens closer to distance of  $2R_{\rm LC}$ . As the pulse propagates outwards and its magnetic field drops as  $\sim 1/r$ , the emission frequency decreases, leading to the downward frequency drift similar to a "sad trombone" effect observed in FRBs [70-72]. This is different from a "trombone" effect caused by orbital decay which will push the flares to higher strengths of the magnetic field on collision with the orbital current sheet, causing the frequency to drift upwards between individual flaring events. We point out that this radio emission is distinct from x-ray transients produced in current sheets behind the flaring bubble with higher field strengths [33]. These would be produced earlier, but would propagate together

with the bubble escaping at relativistic speed and, thus, arrive later to the observer with a delay of  $\sim R_{\rm LC}/c \sim 1$  ms. Using the dissipated power in Fig. 4 as an upper limit, we find X-ray luminosity is expected to be  $L_X \lesssim 4 \times 10^{41}$  erg/s. Last, we have also verified that fast magnetosonic waves excited during the pulse-current sheet interaction can escape the binary magnetosphere and wind as electromagnetic waves. An estimate of these propagation effects is presented in the Appendix.

Discussion.—In this Letter, we have described a novel mechanism to produce FRB-like transients from the late inspiral of neutron star binaries. More specifically, we have shown that the presence of magnetic fields in excess of  $10^{11}G$ , will lead to the production of millisecond radio transients in the frequency range of 10-20 GHz. This is based on identifying large scale interactions of electromagnetic flares with the orbital current sheet of the binary, akin to FRB production mechanisms for active magnetars [50,51]. On the basis of our earlier findings [35,36], we believe this mechanism to be generically applicable to many binary neutron star gravitational wave events provided that the magnetic field orientations of the stellar fields are loosely anti-aligned. For such configurations, electromagnetic flares are being launched periodically from the system (see Ref. [37] for a detailed computation of the period), where flaring to first order will depend on the relative spin rate in the system [56], which can be enhanced for counterspinning neutron stars. Hence, rapidly spinning binaries can produce sub-millisecond pulsations, similar to those observed in transients such as FRB20201020A [60]. Since most FRBs feature emission firmly < 8 GHz (see, e.g., [73] for a recent review), the mechanism proposed here would lead to an undiscovered subpopulation of FRBlike events at higher frequencies. Though, more sophisticated studies of both the emission mechanism in three dimensions and propagation effects in the binary wind will be required to clarify these points. The joint availability of all-sky-coverage at frequencies  $\leq 20$  GHz, e.g., by SKA [74], as well as early warning systems for neutron star coalescence [75–78] might help to put this mechanism to a firm test.

The authors are grateful for discussions with K. Cleary, G. Hallinan, M. Lyutikov, B. Metzger, K. Mooley, J. Nättilä, E. Quataert, and J. Stone. E. R. M. gratefully acknowledges support from a joint fellowship at the Princeton Center for Theoretical Science, the Princeton Gravity Initiative and the Institute for Advanced Study. The simulations were performed on the NSF Frontera supercomputer under Grants AST20008 and AST21006. A. P. acknowledges support by the National Science Foundation under Grant No. AST-1909458. This work was performed in part at the Aspen Center for Physics, which is supported by National Science Foundation grant PHY-1607611, and was facilitated by Multimessenger Plasma Physics Center (MPPC), NSF Grant No. PHY-2206607. E. R. M. also

acknowledges the Extreme Science and Engineering Discovery Environment (XSEDE) [79] through Expanse at SDSC and Bridges-2 at PSC through allocations PHY210053 and PHY210074. E. R. M. further acknowledges the use of computational resources managed and supported by Princeton Research Computing, a consortium of groups including the Princeton Institute for Computational Science and Engineering (PICSciE) and the Office of Information Technology's High Performance Computing Center and Visualization Laboratory at Princeton University. E. R. M. also acknowledges the use of high-performance computing at the Institute for Advanced Study. This work has made extensive use of a number of software packages. Those include AMRex [80], Matplotlib [81], NumPy [82], and SciPy [83].

Appendix A: Methods.—In this Letter, we simulate the global dynamics of the plasma by considering a perfectly conducting electron-positron pair plasma [84] surrounding the two neutron stars [29,31]. Such global dynamics can be well captured using (resistive) forceelectrodynamics approaches (e.g., [52–54]). Building on our earlier work [35,36], we model the binary as two perfectly conducting spheres on a circular orbit. We impose spin on the individual spheres by adjusting the local uniform rotation rate. We exclude precessing motion and only include alignment of the stellar and orbital rotation axes. Overall, we solve the equations of general-relativistic electrodynamics [38,85] using a flat spacetime, which is corotating at the orbital frequency [34,36]. The effects of neglecting the gravitational potential (curved spacetime) are negligible compared to the uncertainties in the emission modeling (see emission section). We model the effects of a forcefree pair plasma [84] using an effective current damping the electric field component parallel to the magnetic field [86], see also [87]. This prescription for the current has been shown to introduce an effective resistive scale into the plasma [88,89], see also [90]. The latter allows us to qualitatively capture reconnection in current sheets present in the simulations. Numerically, these equations are discretized using a fourth-order accurate finitevolume scheme [91] with WENO-Z reconstruction [92] and a Rusanov flux solver [93]. We further utilize the adaptive mesh-refinement infrastructure of the AMReX framework [80]. For the results presented in this work, we have considered two representative binary configurations, both at a separation distance of 52 km. The first one is an irrotational system, with counteroriented dipoles, and a ratio of the field strengths  $B_1 \gg B_2$  at the surfaces of stars 1/2, we choose  $B_1 = 50 \times B_2$ . The second system contains a counterspinning neutron star with spin frequency f = -300 Hzand a magnetic dipole that is inclined by 60° with respect to the stellar spin axis. The other star features a counter-aligned dipole with equal field strengths, i.e.,  $B_1/B_2 = 1$ . While most binary neutron star mergers are not expected to be rapidly spinning [59], we choose a spinning configuration to aid numerical simulation, since spin will affect both the emission period and in our case the location where the flare will interact with the orbital current sheet. The conclusions of our work remain unaffected by this choice. More details about the code and these types of setup can be found in [36].

Appendix B: Propagation effects.—Fast-magnetosonic waves emitted during mergers of magnetic islands in the reconnection layer propagate outwards on top of the magnetic pulse. These waves can be released as radio emission when the pulse is decelerated at the collision with the termination shock of the binary wind. However, several processes can affect their propagation. Because the strength of the magnetic field in the waves remains subdominant compared to the field in the pulse, their conversion to strong shocks [94] and intense scattering by magnetized particles [95] remain inefficient. (Waves produced in the current sheet in the inner magnetosphere will be strongly absorbed by these mechanisms.) Here, we apply the estimates by Lyubarsky [50] performed in the context of reconnection-driven radio bursts from magnetar magnetospheres, since this is the mechanism that we also invoke in the binary.

In order to estimate the propagation effects, we first need to calculate the properties of the binary wind and massloading of the pulse. The particle flux in the wind is  $\dot{N} = \mathcal{M}\mu c/(eR_{\rm LC}^2)$ , where  $\mathcal{M} \sim 10^4$  is the plasma multiplicity (For  $B_* \sim 10^{11}$  G and fast rotation of the binary,  $P \sim 10$  ms, we assume a pulsarlike multiplicity in the magnetosphere, although this point will require a separate investigation.) and  $\mu$  is the magnetic moment of stars. The magnetization parameter of the wind, the ratio of the Poynting flux to the rest mass energy flux, is  $\eta =$  $B_{\rm LC}^2 R_{\rm LC}^2 / (\dot{N} m_e c) \sim (e B_{\rm LC} R_{\rm LC}) / (\mathcal{M} m_e c^2) \sim 5 \times 10^7 [B_{\rm LC} / c]$  $(4 \times 10^7 \text{ G})[(P/4 \text{ ms})(10^4/M)]$ . Starting from the light cylinder, the wind linearly accelerates with distance, until it reaches the magnetosonic surface at  $\sim R_{\rm LC} \eta^{1/3} \sim 7 \times$ 109 cm, beyond which the acceleration is slow [96]. The Lorentz factor of the wind at this distance is  $\gamma_{\rm w}=3\eta^{1/3}\sim 10^3.$  It can further accelerate because of the possible additional magnetic dissipation in the stripes [97].

The pulse picks plasma particles from the inner magnetosphere,  $N \sim M\mu/(eR_{\rm LC})$ , and drags them out. The corresponding magnetization parameter of the pulse beyond the fast magnetosonic surface is  $\sigma_p = E_p/(Nm_ec^2\gamma_w) \sim 3 \times 10^7$ , where  $E_p \sim 10^{39}$  erg is the energy in the pulse. In the frame of the binary the pulse propagates at the Lorentz factor  $\gamma_p = 2\Gamma\gamma_w \sim 6 \times 10^3$  [50].

The magnetization can be lower because of the additional pair production during the interaction of the pulse and magnetospheric stripe close to the light cylinder. The high value of the magnetic compactness parameter

near the reconnection layer at the light cylinder,  $l_B =$  $\sigma_T(B_{\rm flare}/\Gamma)^2 R_{\rm LC}/(8\pi m_e c^2) \sim 10^4$  [51], suggests that enhanced pair production is likely to occur in this regime, which would decrease the pulse magnetization. Note that the value of the magnetic compactness and efficiency of pair creation quickly drops with distance, as the field strength in the flare drops and its Lorentz factor increases. This does not affect the frequencies of emitted fastmagnetosonic waves, because reconnection dynamics remains dominated by synchrotron cooling, as long as  $\gamma_{\rm rad}' = \sqrt{3e\beta_{\rm rec}/(2r_e^2B_{\rm flare}')} \sim 10^3 \ll \sigma_p$ . The pulse also picks up additional magnetic flux,  $\phi \sim \xi B_{\rm LC} R_{\rm LC} R/(2\gamma_w^2)$ , where  $\xi$  < 1 is a dimensionless coefficient which describes the ratio of the mean to the total field in the striped wind, and plasma from the wind. It accumulates in a very thin shell,  $\delta/l = \phi/\phi_{\rm flare} \sim 2 \times 10^{-3} \xi (R/10^{12} \text{ cm})$ , where l = $c\tau$  is the length of the pulse, and does not affect the wave propagation in the body of the pulse at the cyclotron absorption radius (see below).

As the fast-magnetosonic waves propagate outwards, and the magnetic field in the pulse drops, cyclotron absorption can become important. It happens when the wave frequency in the pulse frame,  $\omega'$  matches the particle's gyrofrequency,  $\omega_B' = e B_{\text{pulse}}'/(m_e c)$ . This happens at a distance  $R_c = e \sqrt{\mathcal{L}_{\text{EM}}/c}/(2\pi\nu_{\text{FRB}}m_e c) = 10^{12} \text{ cm}(\mathcal{L}_{\text{EM}}/10^{42} \text{ erg/s})^{1/2}$  (15 GHz/ $\nu_{\text{FRB}}$ ). The optical depth can be calculated as  $\tau_c = \int 4\pi^2 (e^2/m_e c)\delta(\omega' - \omega_B')N'dR'$ , where N' is the pair density in the pulse co-moving frame. Using Eq. (34) in [50], one obtains  $\tau_c \sim \pi^2 \nu_{\text{FRB}} R_c/(\sigma_p \gamma_p^2 c) \sim (10^5/\sigma_p)(6\times 10^3/\gamma_p)^2$ . It means that cyclotron absorption is not important for  $\sigma_p \gtrsim 10^5$ .

Before reaching the cyclotron radius, the fast-magnetosonic waves may steepen into shocks which can lead to their dissipation. In the pulse frame, the steepening can occur at a distance  $\sim\!\!\sigma_p(B'_{\rm pulse}/\delta B')c/\omega'$ . In the binary frame, it corresponds to a distance  $R_s\sim 4\gamma_p^2\sigma_p c(\mathcal{L}_{\rm EM}/\mathcal{L}_{\rm radio})^{1/2}/(2\pi\nu_{\rm FRB})\sim 4\times 10^9\sigma_p$  cm, which is well outside the cyclotron radius for any reasonable value of the pulse magnetization,  $\sigma_p\gtrsim 10^2$ . Thus, the nonlinear wave steepening is negligible.

Another potentially important process is the nonlinear decay of fast-magnetosonic waves into a pair of Alfven waves or into an Alfven and fast wave [50]. In the inner wind zone, the characteristic optical depth,  $\tau_{\rm NL} \sim \int (\delta B'/B'_{\rm pulse})^2 \omega' dr'/c$ , is dominated by the contribution near the light cylinder, when the wind is mildly relativistic. This estimate leads to  $\tau_{\rm NL} \sim (\mathcal{L}_{\rm EM}/\mathcal{L}_{\rm radio})$   $(\omega R_{\rm LC})/(2c\gamma_p^2) \sim 50$ , where  $\gamma_p \sim 5$  near the light cylinder. However, two important things may prevent efficient conversion into Alfven waves. First, since they propagate along the magnetic field, there are no pre-existing Alfven waves in the wind zone. In order for the interaction to be efficient, Alfven waves need to grow from noise, which

requires substantial optical depth,  $\sim$ 10. Second, the above estimate is an upper limit, since the nonlinear interaction of fast and Alfven waves decreases in the oblique limit,  $k_{\perp}/k_{\parallel} > 1$  [98]. To summarize, we expect only modest effects of nonlinear conversion processes on the wave propagation near the light cylinder. Beyond the fast magnetosonic radius, the optical depth may increase again,  $\tau_{\rm NL} \sim (\mathcal{L}_{\rm radio}/\mathcal{L}_{\rm EM})(\omega R)/(2c\gamma_p^2) \sim R/(2\times 10^{11} {\rm cm})$ , which is nominally significant beyond the cyclotron radius. However, at that distance the wave frequency exceeds the plasma frequency,  $\omega'/\omega'_p = \sqrt{\sigma_p}\omega'/\omega'_B =$  $\sqrt{\sigma_p}(R/R_c) \gg 1$ , Alfven waves do not exist and the nonlinear interaction is absent. Finally, beyond the cyclotron radius induced scattering can be important. The estimate by [50] shows  $\tau_s \sim [1/(\sigma_p \gamma_p^2)](\mathcal{L}_{\text{radio}}/\mathcal{L}_{\text{EM}})$  $(\omega_B/\omega)^4 (\omega R/c) \sim 10\sigma_p^{-1} (10^{12} \text{ cm/}R)^3$ , which is negligible for  $\sigma_p \gtrsim 10$ .

## \*emost@princeton.edu

- [1] B. P. Abbott *et al.* (LIGO Scientific and Virgo Collaborations), GW170817: Observation of Gravitational Waves from a Binary Neutron Star Inspiral, Phys. Rev. Lett. **119**, 161101 (2017).
- [2] B. P. Abbott *et al.* (LIGO Scientific and Virgo Collaborations), GW190425: Observation of a compact binary coalescence with total mass  $\sim 3.4 M_{\odot}$ , Astrophys. J. Lett. **892**, L3 (2020).
- [3] B. P. Abbott et al. (LIGO Scientific, Virgo, Fermi GBM, INTEGRAL, IceCube, AstroSat Cadmium Zinc Telluride Imager Team, IPN, Insight-Hxmt, ANTARES, Swift, AGILE Team, 1M2H Team, Dark Energy Camera GW-EM, DES, DLT40, GRAWITA, Fermi-LAT, ATCA, AS-KAP, OzGrav, DWF (Deeper Wider Faster Program), AST3, CAASTRO, VINROUGE, MASTER, J-GEM, GROWTH, JAGWAR, CaltechNRAO, TTU-NRAO, NuSTAR, Pan-STARRS, MAXI Team, TZAC Consortium, KU, Nordic Optical Telescope, ePESSTO, GROND, Texas Tech University, TOROS, BOOTES, MWA, CALET, IKI-GW Follow-up, H.E.S.S., LOFAR, LWA, HAWC, Pierre Auger, ALMA, Euro VLBI Team, Pi of Sky, Chandra Team at McGill University, DFN, ATLAS Telescopes, High Time Resolution Universe Survey, RIMAS, RATIR, SKA South Africa/MeerKAT Collaborations, Las Cumbres Observatory Group, and SALT Group), Multi-messenger observations of a binary neutron star merger, Astrophys. J. Lett. 848, L12 (2017).
- [4] M. M. Kasliwal *et al.*, Illuminating gravitational waves: A concordant picture of photons from a neutron star merger, Science 358, 1559 (2017).
- P. S. Cowperthwaite *et al.*, The electromagnetic counterpart of the binary neutron star merger LIGO/Virgo GW170817.
   II. UV, optical, and near-infrared light curves and comparison to kilonova models, Astrophys. J. Lett. 848, L17 (2017).
- [6] R. Chornock et al., The electromagnetic counterpart of the binary neutron star merger LIGO/VIRGO GW170817.
  IV. Detection of near-infrared signatures of r-process

- nucleosynthesis with gemini-south, Astrophys. J. Lett. **848**, L19 (2017).
- [7] V. A. Villar *et al.*, The combined ultraviolet, optical, and near-infrared light curves of the kilonova associated with the binary neutron star merger GW170817: Unified data set, analytic models, and physical implications, Astrophys. J. Lett. **851**, L21 (2017).
- [8] M. Nicholl *et al.*, The electromagnetic counterpart of the binary neutron star merger LIGO/VIRGO GW170817.
   III. Optical and UV spectra of a blue kilonova from fast polar ejecta, Astrophys. J. Lett. 848, L18 (2017).
- [9] E. Troja, L. Piro, G. Ryan, H. van Eerten, R. Ricci, M. Wieringa, S. Lotti, T. Sakamoto, and S. B. Cenko, The outflow structure of GW170817 from late-time broad-band observations, Mon. Not. R. Astron. Soc. 478, L18 (2018).
- [10] N. R. Tanvir *et al.*, The emergence of a lanthanide-rich kilonova following the merger of two neutron stars, Astrophys. J. Lett. **848**, L27 (2017).
- [11] M. R. Drout *et al.*, Light curves of the neutron star merger GW170817/SSS17a: Implications for R-process nucleosynthesis, Science 358, 1570 (2017).
- [12] B. P. Abbott *et al.* (LIGO Scientific, Virgo, Fermi-GBM, and INTEGRAL Collaborations), Gravitational waves and gamma-rays from a binary neutron star merger: GW170817 and GRB 170817A, Astrophys. J. Lett. 848, L13 (2017).
- [13] V. Savchenko *et al.*, INTEGRAL detection of the first prompt gamma-ray signal coincident with the gravitational-wave event GW170817, Astrophys. J. Lett. **848**, L15 (2017).
- [14] E. Troja *et al.*, The x-ray counterpart to the gravitational wave event GW 170817, Nature (London) **551**, 71 (2017).
- [15] R. Margutti *et al.*, The electromagnetic counterpart of the binary neutron star merger LIGO/VIRGO GW170817. V. Rising x-ray emission from an off-axis jet, Astrophys. J. Lett. **848**, L20 (2017).
- [16] R. Margutti *et al.*, The binary neutron star event LIGO/Virgo GW170817 160 days after merger: Synchrotron emission across the electromagnetic spectrum, Astrophys. J. Lett. **856**, L18 (2018).
- [17] A. Hajela *et al.*, Two years of nonthermal emission from the binary neutron star merger GW170817: Rapid fading of the jet afterglow and first constraints on the kilonova fastest ejecta, Astrophys. J. Lett. **886**, L17 (2019).
- [18] G. Hallinan et al., A radio counterpart to a neutron star merger, Science 358, 1579 (2017).
- [19] K. D. Alexander et al., The electromagnetic counterpart of the binary neutron star merger LIGO/VIRGO GW170817. VI. Radio constraints on a relativistic jet and predictions for late-time emission from the kilonova ejecta, Astrophys. J. Lett. 848, L21 (2017).
- [20] G. Ghirlanda *et al.*, Compact radio emission indicates a structured jet was produced by a binary neutron star merger, Science 363, 968 (2019).
- [21] K. P. Mooley *et al.*, A mildly relativistic wide-angle outflow in the neutron star merger GW170817, Nature (London) **554**, 207 (2018).
- [22] K. P. Mooley, A. T. Deller, O. Gottlieb, E. Nakar, G. Hallinan, S. Bourke, D. A. Frail, A. Horesh, A. Corsi, and K. Hotokezaka, Superluminal motion of a relativistic jet in the neutron-star merger GW170817, Nature (London) 561, 355 (2018).

- [23] B. D. Metzger, Kilonovae, Living Rev. Relativity 23, 1 (2020).
- [24] D. Radice, S. Bernuzzi, and A. Perego, The dynamics of binary neutron star mergers and GW170817, Annu. Rev. Nucl. Part. Sci. 70, 95 (2020).
- [25] S. Xiao et al., The quasi-periodically oscillating precursor of a long gamma-ray burst from a binary neutron star merger, arXiv:2205.02186.
- [26] D. Tsang, J. S. Read, T. Hinderer, A. L. Piro, and R. Bondarescu, Resonant Shattering of Neutron Star Crusts, Phys. Rev. Lett. 108, 011102 (2012).
- [27] B. D. Metzger and C. Zivancev, Pair fireball precursors of neutron star mergers, Mon. Not. R. Astron. Soc. 461, 4435 (2016).
- [28] Z. Zhang, S.-X. Yi, S.-N. Zhang, S.-L. Xiong, and S. Xiao, Tidally-induced magnetar super flare at the eve of coalescence with its compact companion, Astrophys. J. Lett. 939, L25 (2022).
- [29] B. M. S. Hansen and M. Lyutikov, Radio and x-ray signatures of merging neutron stars, Mon. Not. R. Astron. Soc. 322, 695 (2001).
- [30] J.-S. Wang, Y.-P. Yang, X.-F. Wu, Z.-G. Dai, and F.-Y. Wang, Fast radio bursts from the inspiral of double neutron stars, Astrophys. J. Lett. 822, L7 (2016).
- [31] M. Lyutikov, Electrodynamics of binary neutron star mergers, Mon. Not. R. Astron. Soc. 483, 2766 (2019).
- [32] N. Sridhar, J. Zrake, B. D. Metzger, L. Sironi, and D. Giannios, Shock-powered radio precursors of neutron star mergers from accelerating relativistic binary winds, Mon. Not. R. Astron. Soc. 501, 3184 (2021).
- [33] A. M. Beloborodov, Emission of magnetar bursts and precursors of neutron star mergers, Astrophys. J. 921, 92 (2021).
- [34] F. Carrasco and M. Shibata, Magnetosphere of an orbiting neutron star, Phys. Rev. D **101**, 063017 (2020).
- [35] E. R. Most and A. A. Philippov, Electromagnetic precursors to gravitational wave events: Numerical simulations of flaring in pre-merger binary neutron star magnetospheres, Astrophys. J. Lett. 893, L6 (2020).
- [36] E. R. Most and A. A. Philippov, Electromagnetic precursor flares from the late inspiral of neutron star binaries, Mon. Not. R. Astron. Soc. **515**, 2710 (2022).
- [37] S. A. Cherkis and M. Lyutikov, Magnetic topology in coupled binaries, spin-orbital resonances, and flares, Astrophys. J. **923**, 13 (2021).
- [38] C. Palenzuela, L. Lehner, M. Ponce, S. L. Liebling, M. Anderson, D. Neilsen, and P. Motl, Electromagnetic and Gravitational Outputs from Binary-Neutron-Star Coalescence, Phys. Rev. Lett. 111, 061105 (2013).
- [39] C. Palenzuela, L. Lehner, S. L. Liebling, M. Ponce, M. Anderson, D. Neilsen, and P. Motl, Linking electromagnetic and gravitational radiation in coalescing binary neutron stars, Phys. Rev. D 88, 043011 (2013).
- [40] M. Ponce, C. Palenzuela, E. Barausse, and L. Lehner, Electromagnetic outflows in a class of scalar-tensor theories: Binary neutron star coalescence, Phys. Rev. D **91**, 084038 (2015).
- [41] A. Nathanail, A toy model for the electromagnetic output of neutron-star merger prompt collapse to a black hole: Magnetized neutron-star collisions Astrophys. J. 892, 35 (2020).

- [42] L. Lehner, C. Palenzuela, S. L. Liebling, C. Thompson, and C. Hanna, Intense electromagnetic outbursts from collapsing hypermassive neutron stars, Phys. Rev. D 86, 104035 (2012).
- [43] C. Palenzuela, Modeling magnetized neutron stars using resistive MHD, Mon. Not. R. Astron. Soc. 431, 1853 (2013).
- [44] K. Dionysopoulou, D. Alic, C. Palenzuela, L. Rezzolla, and B. Giacomazzo, General-relativistic resistive magnetohydrodynamics in three dimensions: Formulation and tests, Phys. Rev. D 88, 044020 (2013).
- [45] E. R. Most, A. Nathanail, and L. Rezzolla, Electromagnetic emission from blitzars and its impact on non-repeating fast radio bursts, Astrophys. J. **864**, 117 (2018).
- [46] A. Bransgrove, B. Ripperda, and A. Philippov, Magnetic Hair and Reconnection in Black Hole Magnetospheres, Phys. Rev. Lett. **127**, 055101 (2021).
- [47] V. Paschalidis, Z. B. Etienne, and S. L. Shapiro, General relativistic simulations of binary black hole-neutron stars: Precursor electromagnetic signals, Phys. Rev. D 88, 021504(R) (2013).
- [48] W. E. East, L. Lehner, S. L. Liebling, and C. Palenzuela, Multimessenger signals from black hole–neutron star mergers without significant tidal disruption, Astrophys. J. Lett. **912**, L18 (2021).
- [49] F. Carrasco, M. Shibata, and O. Reula, Magnetospheres of black hole-neutron star binaries, Phys. Rev. D 104, 063004 (2021).
- [50] Y. Lyubarsky, Fast radio bursts from reconnection in a magnetar magnetosphere, Astrophys. J. 897, 1 (2020).
- [51] J. F. Mahlmann, A. A. Philippov, A. Levinson, A. Spitkovsky, and H. Hakobyan, Electromagnetic fireworks: Fast radio bursts from rapid reconnection in the compressed magnetar wind, Astrophys. J. Lett. 932, L20 (2022).
- [52] C. Palenzuela, L. Lehner, and S. L. Liebling, Dual jets from binary black holes, Science 329, 927 (2010).
- [53] K. Parfrey, A. M. Beloborodov, and L. Hui, Dynamics of strongly twisted relativistic magnetospheres, Astrophys. J. 774, 92 (2013).
- [54] F. Carrasco, D. Viganò, C. Palenzuela, and J. A. Pons, Triggering magnetar outbursts in 3D force-free simulations, Mon. Not. R. Astron. Soc. 484, L124 (2019).
- [55] A. L. Piro, Magnetic interactions in coalescing neutron star binaries, Astrophys. J. 755, 80 (2012).
- [56] D. Lai, DC circuit powered by orbital motion: Magnetic interactions in compact object binaries and exoplanetary systems, Astrophys. J. Lett. **757**, L3 (2012).
- [57] Y. Lyubarsky, Radio emission of the Crab and Crab-like pulsars, Mon. Not. R. Astron. Soc. **483**, 1731 (2019).
- [58] A. Philippov, D. A. Uzdensky, A. Spitkovsky, and B. Cerutti, Pulsar radio emission mechanism: Radio nanoshots as a low frequency afterglow of relativistic magnetic reconnection, Astrophys. J. Lett. 876, L6 (2019).
- [59] L. Bildsten and C. Cutler, Tidal interactions of inspiraling compact binaries, Astrophys. J. **400**, 175 (1992).
- [60] I. Pastor-Marazuela *et al.*, A fast radio burst with sub-millisecond quasi-periodic structure, arXiv:2202.08002.
- [61] T. A. Callister, M. M. Anderson, G. Hallinan, L. R. D'addario, J. Dowell, N. E. Kassim, T. J. W. Lazio, D. C. Price, and F. K. Schinzel, A first search for prompt radio emission from a gravitational-wave event, Astrophys. J. Lett. 877, L39 (2019).

- [62] See Supplemental Material at http://link.aps.org/supplemental/ 10.1103/PhysRevLett.130.245201 for more details.
- [63] N. F. Loureiro, A. A. Schekochihin, and S. C. Cowley, Instability of current sheets and formation of plasmoid chains, Phys. Plasmas 14, 100703 (2007).
- [64] A. Bhattacharjee, Y.-M. Huang, H. Yang, and B. Rogers, Fast reconnection in high-Lundquist-number plasmas due to the plasmoid Instability, Phys. Plasmas 16, 112102 (2009).
- [65] L. Sironi and A. Spitkovsky, Relativistic reconnection: An efficient source of non-thermal particles, Astrophys. J. Lett. 783, L21 (2014).
- [66] F. Guo, Y.-H. Liu, W. Daughton, and H. Li, Particle acceleration and plasma dynamics during magnetic reconnection in the magnetically-dominated regime, Astrophys. J. 806, 167 (2015).
- [67] F. Guo, X. Li, W. Daughton, H. Li, P. Kilian, Y.-H. Liu, Q. Zhang, and H. Zhang, Magnetic energy release, plasma dynamics, and particle acceleration in relativistic turbulent magnetic reconnection, Astrophys. J. 919, 111 (2021).
- [68] S. Du, H. Li, X. Fu, Z. Gan, and S. Li, Magnetic energy conversion in magnetohydrodynamics: Curvature relaxation and perpendicular expansion of magnetic fields, Astrophys. J. 925, 128 (2022).
- [69] O. French, F. Guo, Q. Zhang, and D. Uzdensky, Particle injection and nonthermal particle acceleration in relativistic magnetic reconnection, arXiv:2210.08358.
- [70] J. W. T. Hessels *et al.*, FRB 121102 bursts show complex time–frequency structure, Astrophys. J. Lett. 876, L23 (2019).
- [71] A. Josephy *et al.*, CHIME/FRB detection of the original repeating fast radio burst source FRB 121102, Astrophys. J. Lett. **882**, L18 (2019).
- [72] F. Rajabi, M. A. Chamma, C. M. Wyenberg, A. Mathews, and M. Houde, A simple relationship for the spectro-temporal structure of bursts from FRB 121102, Mon. Not. R. Astron. Soc. 498, 4936 (2020).
- [73] E. Petroff, J. W. T. Hessels, and D. R. Lorimer, Fast radio bursts at the dawn of the 2020s, Astron. Astrophys. Rev. 30, 2 (2022).
- [74] A. Weltman *et al.*, Fundamental physics with the Square Kilometre Array, Pub. Astron. Soc. Aust. **37**, e002 (2020).
- [75] C. W. James, G. E. Anderson, L. Wen, J. Bosveld, Q. Chu, M. Kovalam, T. J. Slaven-Blair, and A. Williams, Using negative-latency gravitational wave alerts to detect prompt radio bursts from binary neutron star mergers with the Murchison Widefield Array, Mon. Not. R. Astron. Soc. 489, L75 (2019).
- [76] S. Sachdev *et al.*, An early-warning system for electromagnetic follow-up of gravitational-wave events, Astrophys. J. Lett. **905**, L25 (2020).
- [77] Z. Wang, T. Murphy, D. L. Kaplan, K. W. Bannister, and D. Dobie, The capability of the Australian Square Kilometre Array Pathfinder to detect prompt radio bursts from neutron star mergers, Pub. Astron. Soc. Aust. 37, e051 (2020).
- [78] H. Yu, R. X. Adhikari, R. Magee, S. Sachdev, and Y. Chen, Early warning of coalescing neutron-star and neutronstar-black-hole binaries from the nonstationary noise background using neural networks, Phys. Rev. D 104, 062004 (2021)
- [79] J. Towns *et al.*, XSEDE: Accelerating scientific discovery, Comput. Sci. Eng. 16, 62 (2014).
- [80] W. Zhang, A. Almgren, V. Beckner, J. Bell, J. Blaschke, C. Chan, M. Day, B. Friesen, K. Gott, D. Graves, M. Katz,

- A. Myers, T. Nguyen, A. Nonaka, M. Rosso, S. Williams, and M. Zingale, AMReX: A framework for block-structured adaptive mesh refinement, J. Open Source Softwaare 4, 1370 (2019).
- [81] J. D. Hunter, Matplotlib: A 2d graphics environment, Comput. Sci. Eng. 9, 90 (2007).
- [82] C. R. Harris et al., Array programming with NumPy, Nature (London) 585, 357 (2020).
- [83] P. Virtanen *et al.* (SciPy 1.0 Contributors), SciPy 1.0: Fundamental algorithms for scientific computing in PYTHON, Nat. Methods 17, 261 (2020).
- [84] P. Goldreich and W. H. Julian, Pulsar electrodynamics, Astrophys. J. 157, 869 (1969).
- [85] T. W. Baumgarte and S. L. Shapiro, General—relativistic MHD for the numerical construction of dynamical space times, Astrophys. J. 585, 921 (2003).
- [86] D. Alic, P. Mosta, L. Rezzolla, O. Zanotti, and J. L. Jaramillo, Accurate simulations of binary black-hole mergers in force-free electrodynamics, Astrophys. J. 754, 36 (2012).
- [87] A. Spitkovsky, Time-dependent force-free pulsar magnetospheres: Axisymmetric and oblique rotators, Astrophys. J. Lett. 648, L51 (2006).
- [88] B. Ripperda, J. F. Mahlmann, A. Chernoglazov, J. M. TenBarge, E. R. Most, J. Juno, Y. Yuan, A. A. Philippov, and A. Bhattacharjee, Weak Alfvénic turbulence in relativistic plasmas II: Current sheets and dissipation, J. Plasma Phys. 87, 905870512 (2021).
- [89] J. F. Mahlmann and M. A. Aloy, Diffusivity in force-free simulations of global magnetospheres, Mon. Not. R. Astron. Soc. **509**, 1504 (2021).
- [90] J. Li, A. Spitkovsky, and A. Tchekhovskoy, Resistive solutions for pulsar magnetospheres, Astrophys. J. **746**, 60 (2012).
- [91] P. McCorquodale and P. Colella, A high-order finite-volume method for conservation laws on locally refined grids, Commun. Appl. Math. Comput. Sci. 6, 1 (2011).
- [92] R. Borges, M. Carmona, B. Costa, and W. Don, An improved weighted essentially non-oscillatory scheme for hyperbolic conservation laws, J. Comput. Phys. 227, 3191 (2008).
- [93] V. V. Rusanov, Calculation of interaction of non-steady shock waves with obstacles, J. Comput. Math. Phys. USSR 1, 267 (1961).
- [94] A. M. Beloborodov, Monster radiative shocks in the perturbed magnetospheres of neutron stars, arXiv:2210.13509.
- [95] A. M. Beloborodov, Scattering of Ultrastrong Electromagnetic Waves by Magnetized Particles, Phys. Rev. Lett. 128, 255003 (2022).
- [96] V. S. Beskin, I. V. Kuznetsova, and R. R. Rafikov, On the MHD effects on the force-free monopole outflow, Mon. Not. R. Astron. Soc. 299, 341 (1998).
- [97] Y. Lyubarsky and J. G. Kirk, Reconnection in a striped pulsar wind, Astrophys. J. **547**, 437 (2001).
- [98] J. M. TenBarge, B. Ripperda, A. Chernoglazov, A. Bhattacharjee, J. F. Mahlmann, E. R. Most, J. Juno, Y. Yuan, and A. A. Philippov, Weak Alfvénic turbulence in relativistic plasmas. Part 1. Dynamical equations and basic dynamics of interacting resonant triads, J. Plasma Phys. 87, 905870614 (2021).